Synthesis of Supramolecular Fullerene-Porphyrin-Cu(phen)$_2$-Ferrocene Architectures. A Heteroleptic Approach Towards Tetrads

Michael Schmittel,*[a] Ravuri S. K. Kishore,[a] and Jan W. Bats[b]

Supporting Material

1. NMR
2. ESI MS
3. CV and DPV
4. UV
5. Crystal Packing of **5**
6. PM3 structure

1. NMR

Table S 1 ^{1}H NMR shifts of ligands **1-4** measured in CD_2Cl_2

	Por-Hβ	**4-H**	**7-H**	**Ar-Hb, Hb'**	**5-H, 6-H**	**8-H**	**Ar-Ha,Ha')**	**3'''-, 5'''-H**
1	8.84 (d,2H, -$H_{β1}$), 8.75 (d, 2H, $H_{β2}$), 8.70 (s, 4H, $H_{β3}$, $H_{β4}$)	8.66 (s)	8.36 (d)	8.16(d)	7.97 (br s)	7.61(d)	7.51(d)	6.98 (s)
2	8.93 (s, 2H, $H_{β1}$), 8.88 (d, 2H, $H_{β2}$), 8.80 (d, 2H, $H_{β3}$), 8.75 (s, 2H, $H_{β4}$),	8.66 (s)	8.33 (d)	8.17(d)	7.92 (br. s)	7.59 (d)	7.55 (d)	7.00(s)
3	8.77 (d, 4H, $H_{β1}$), 8.67 (d, 4H, $H_{β2}$),	8.65 (s)	8.36 (d)	8.13(d)	7.96(br s)	7.58(d)	7.47(d)	6.96(s)
4	8.93 (s, 8H, $H_β$)	8.63 (s)	8.32 (d)	8.13(d)	7.89 (br s)	7.60 (d)	7.53(d)	6.98 (s)

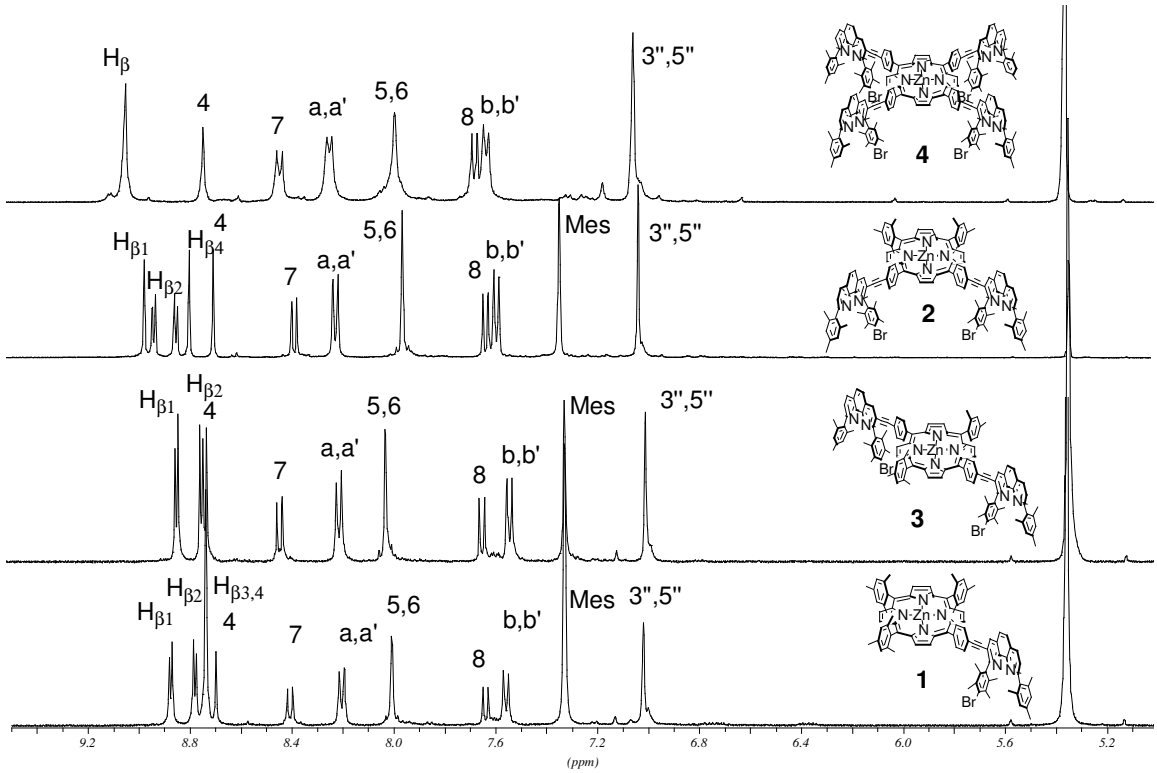

Figure S 1 Aromatic region (^{1}H NMR) of ligands **1-4** displaying the various shifts for the porphyrin and phenanthroline protons in CD_2Cl_2.

Table S 2 NMR shifts (^{1}H NMR) of **6-14** measured in CD_2Cl_2 (**6-9**) or in 1:1 CD_2Cl_2/CS_2 (**11-14**)

	Por-Hβ	**4-H**	**7-H**	**3'''-, 5'''-H**	**Fc**	**Py 3''-, 5''-H**	**Pyr-H5a, -H5b, -H2**
6	8.74(d), 8.69(d), 8.65(s)	8.99	8.78	6.15	4.58, 4.35, 4.26		
7	8.77(s), 8.74(d), 8.71(d), 8.68	9.00	8.79	6.15	4.66, 4.43, 4.34		
8	8.76 (d), 8.70 (d)	8.98	8.77	6.14	4.72, 4.46, 4.41		
9	8.76	8.99	8.77	6.14	4.66, 4.43, 4.34		
11	8.64(d), 8.58(d), 8.55(s)	8.97	8.83(d)	6.21	4.58, 4.36, 4.27	6.45 (br s)	4.66(d), 4.56 (s), 3.93(d)
12	8.66(d), 8.65 (s), 8.59 (d), 8.56 (s)	8.97	8.83	6.21	4.58, 4.35, 4.26	6.26 (br s)	4.36 (s), 4.22(d)
13	8.65 (d), 8.59 (d)	8.98	8.83	6.20	4.60, 4.39, 4.29	6.22(br, s)	4.57(d), 4.45 (s), 3.83(d)
14	8.67	8.99	8.79	6.18	4.62, 4.39, 4.30	6.23 (br, s)	4.77(d), 4.46 (s), 3.95(d)

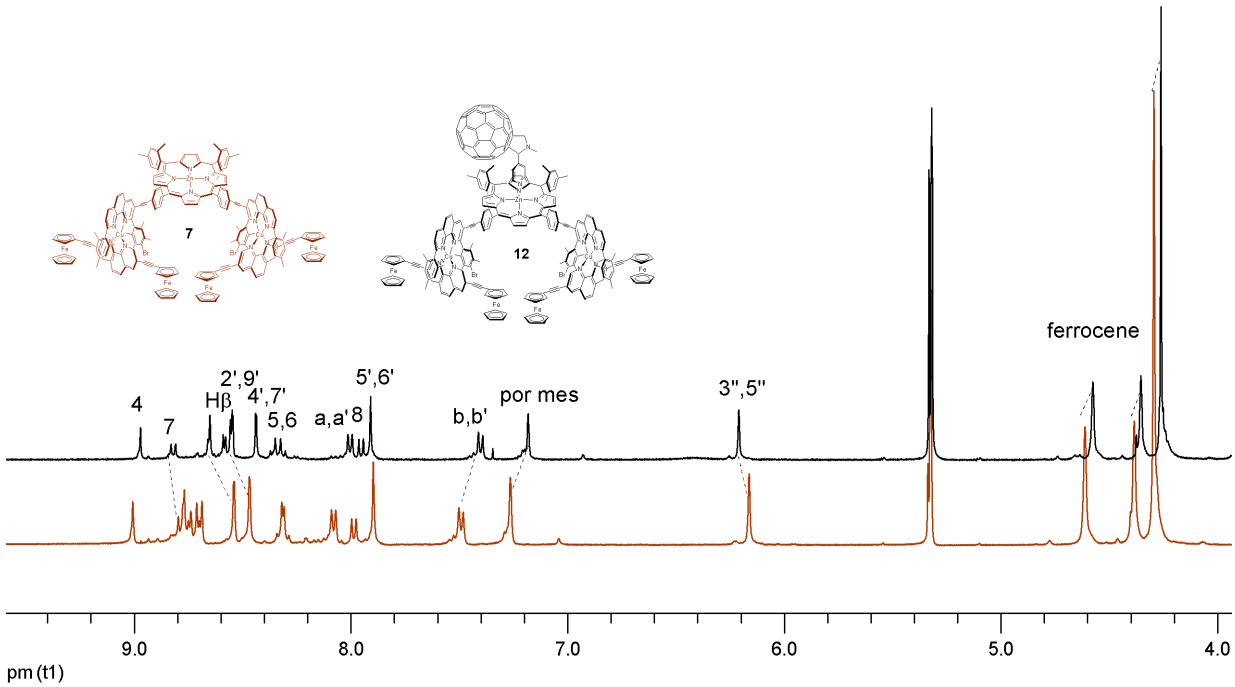

Figure S 2 Comparison of the aromatic region in the ^{1}H NMR of **7** and **12**. The shifts are marked by dotted lines.

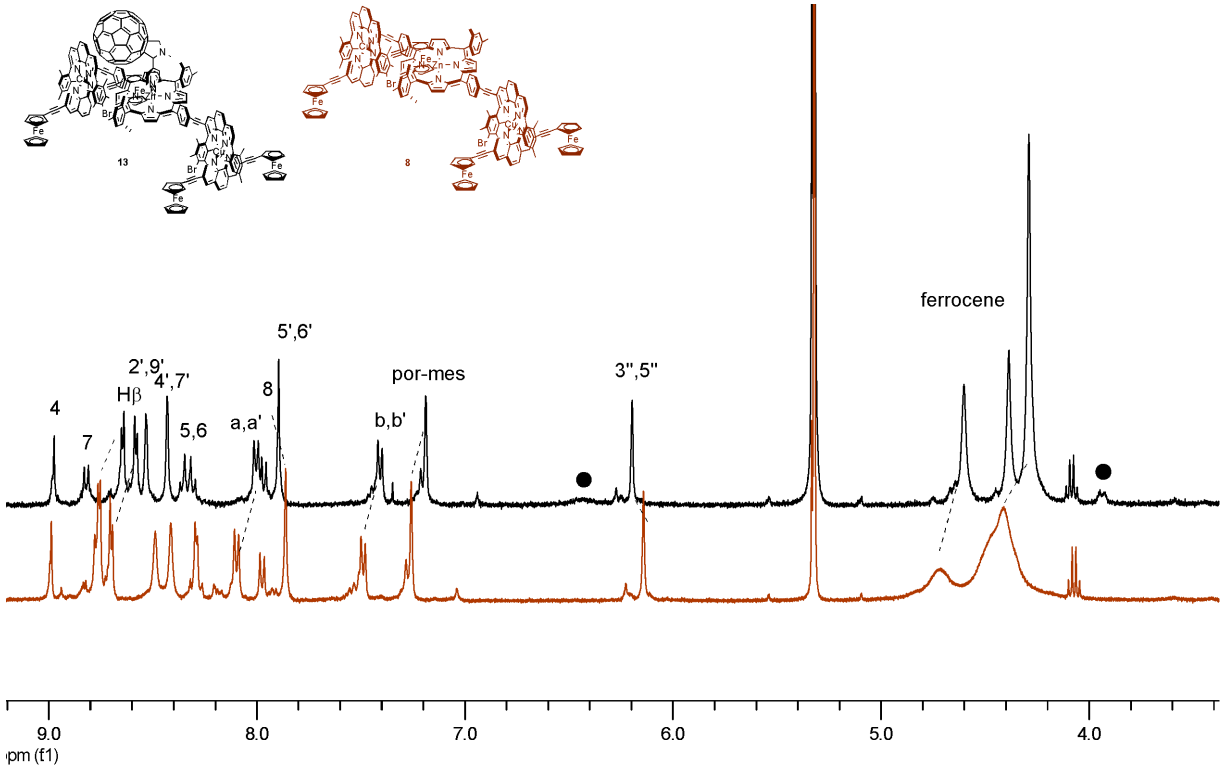

Figure S 3 Comparison of the aromatic region in the ^{1}H NMR of **8** and **13**. The shifts are marked by dotted lines. The black dots represent the upfield shifted signals of the pyridyl group at C_{60}

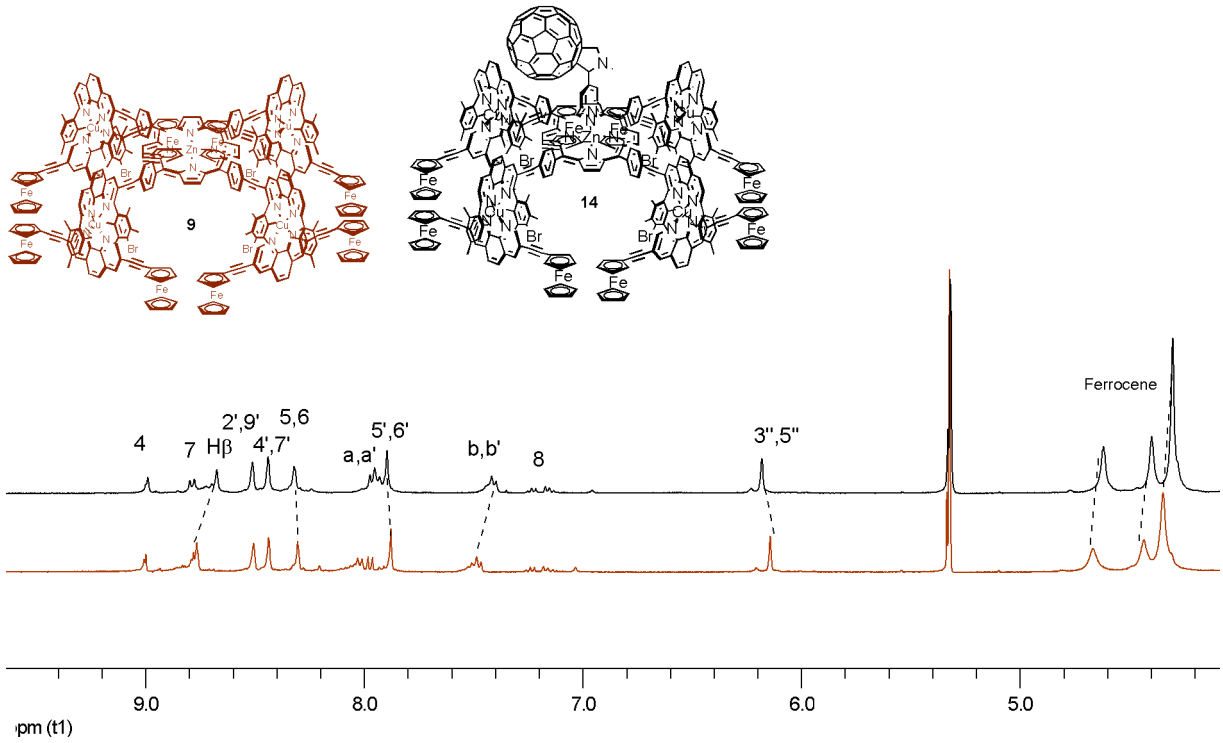

Figure S 4 Comparison of the aromatic region in the ^{1}H NMR of **9** and **14**. The shifts are marked by dotted lines.

2. ESI- MS

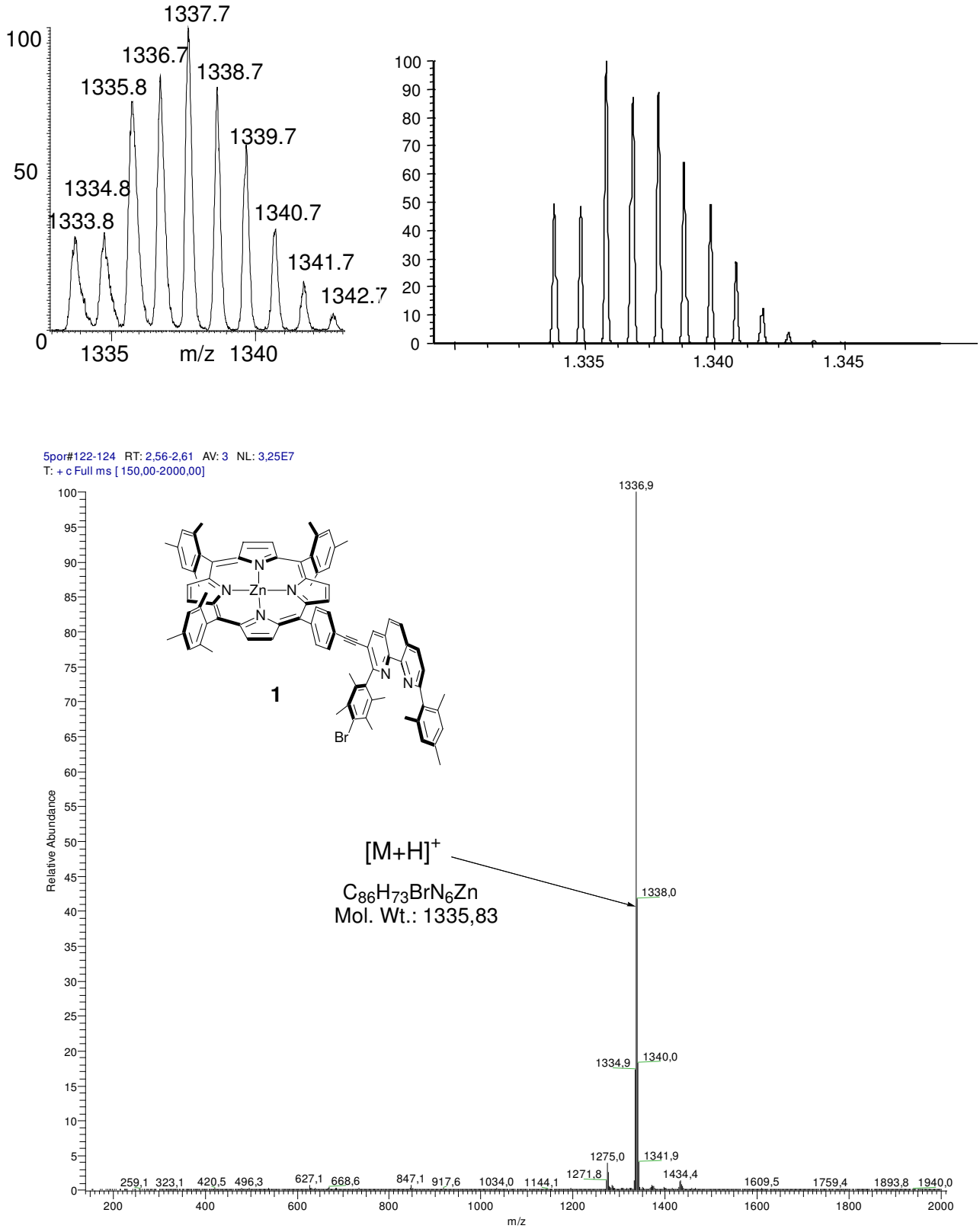

Figure S 5 ESI-MS of **1** showing a $[M+H]^+$ signal at about m/z = 1337. Top left: isotopic splitting pattern recorded for **1**. Top right: Simulated isotopic splitting pattern.

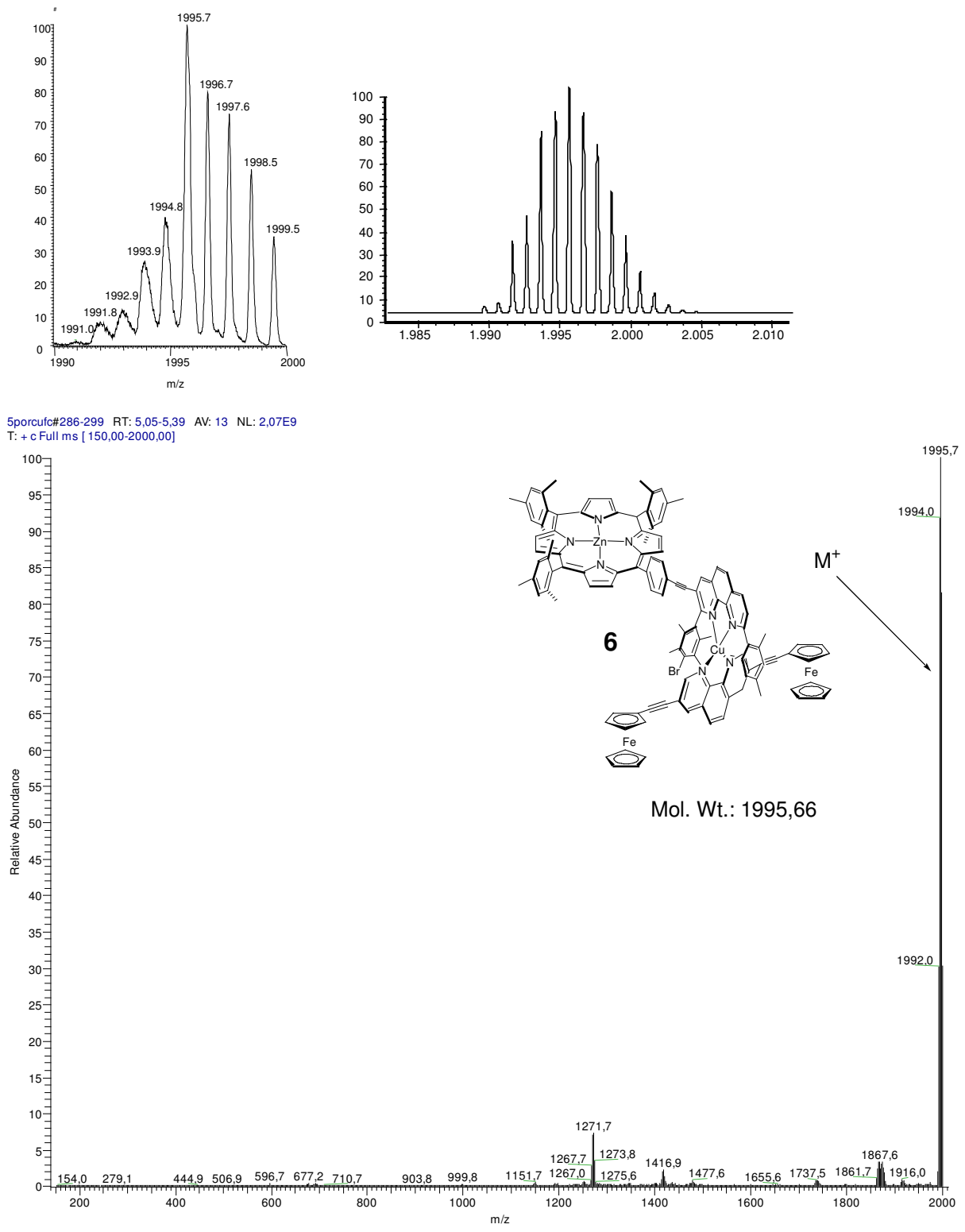

Figure S 6 ESI-MS of **6** showing the M^+ signal at about m/z = 1995. Top left: isotopic splitting pattern recorded for **6**. Top right: Simulated isotopic splitting pattern.

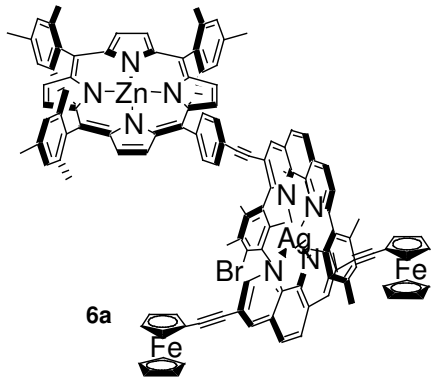

6a

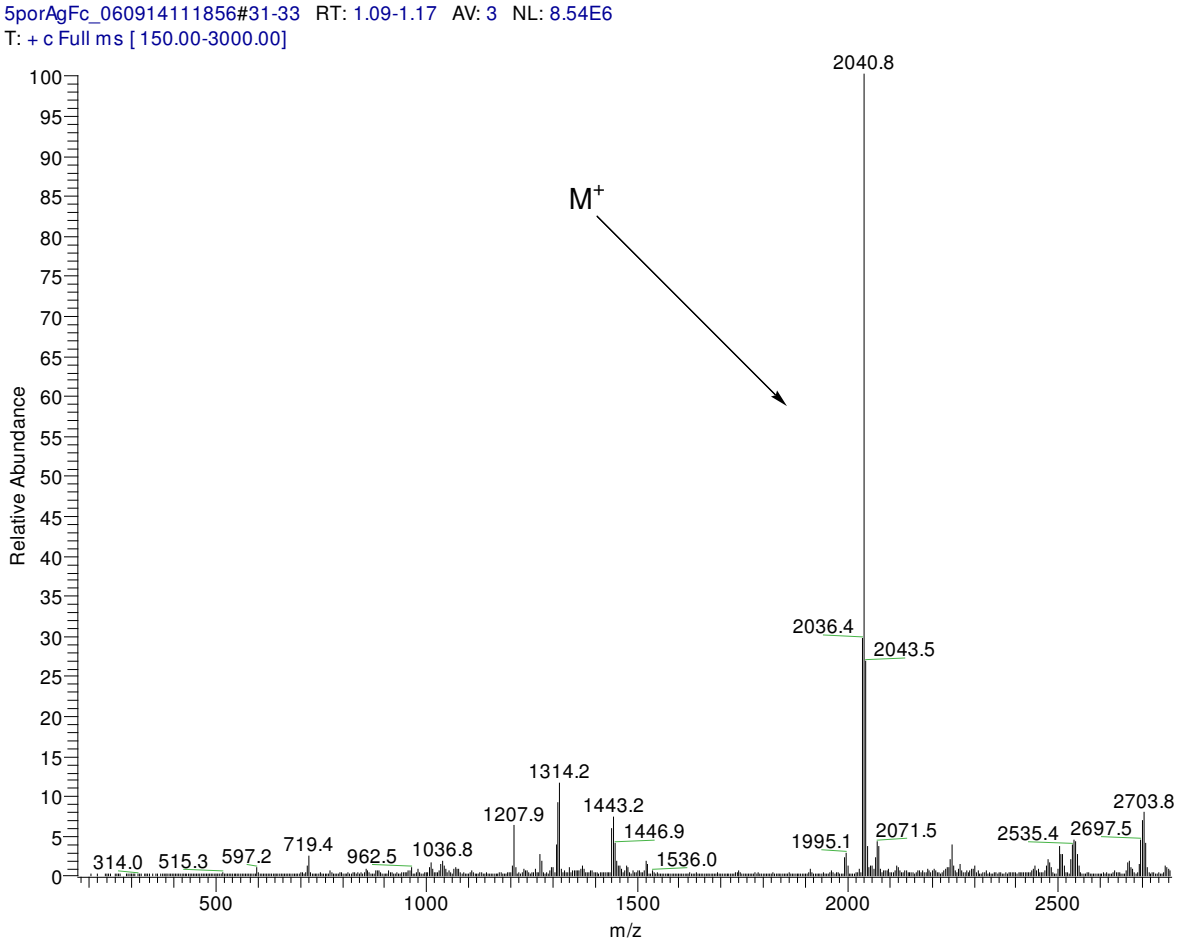

Figure S 7 ESI-MS of **6a** showing the M^+ signal at about m/z = 2040.

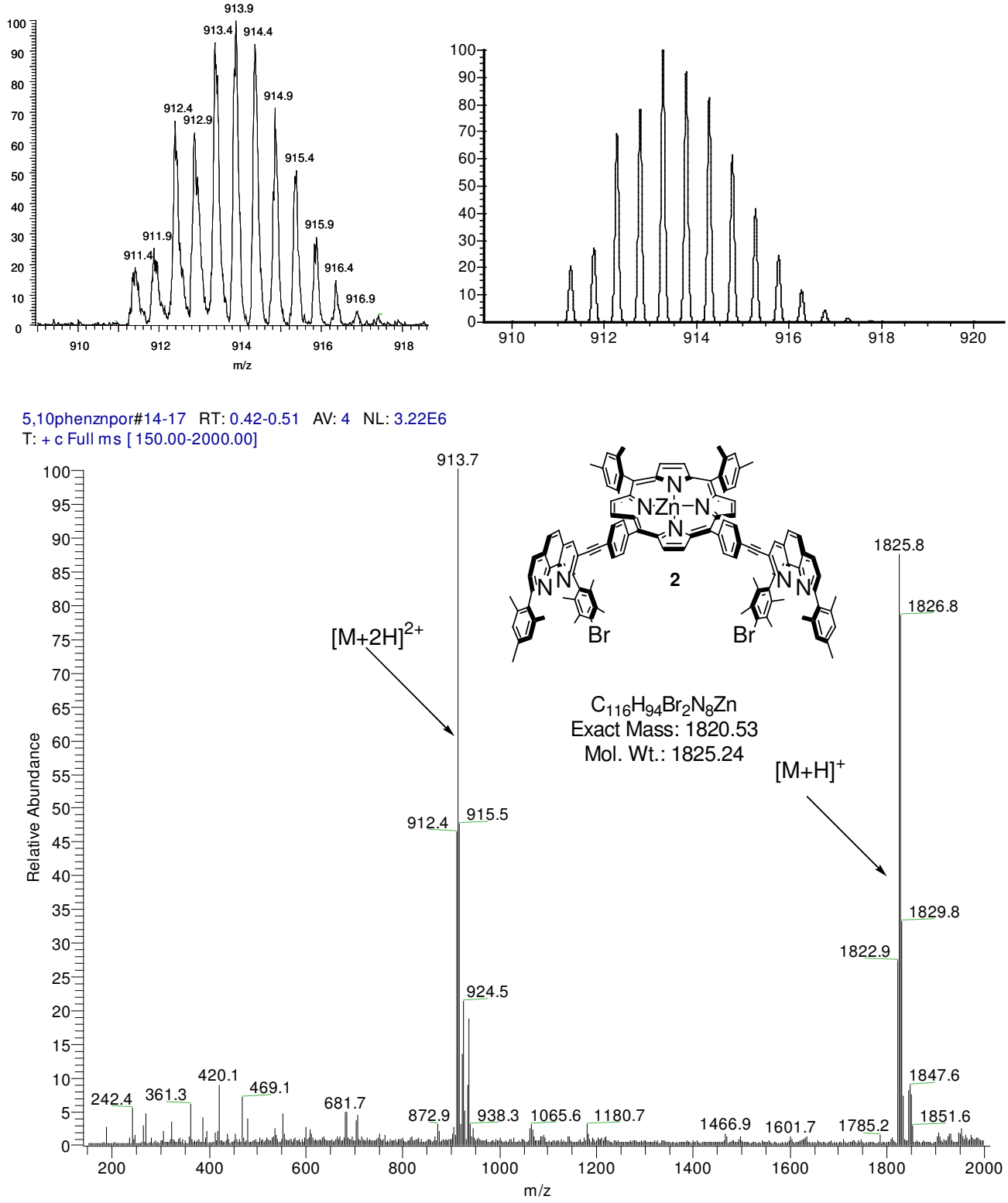

Figure S 8 ESI-MS of **2** showing the $[M+H]^+$ and $[M+2H]^{2+}$ signals. Top left: isotopic splitting pattern recorded for $[M+H]^{2+}$ of **2**. Top right: Simulated isotopic splitting pattern for $[M+H]^{2+}$.

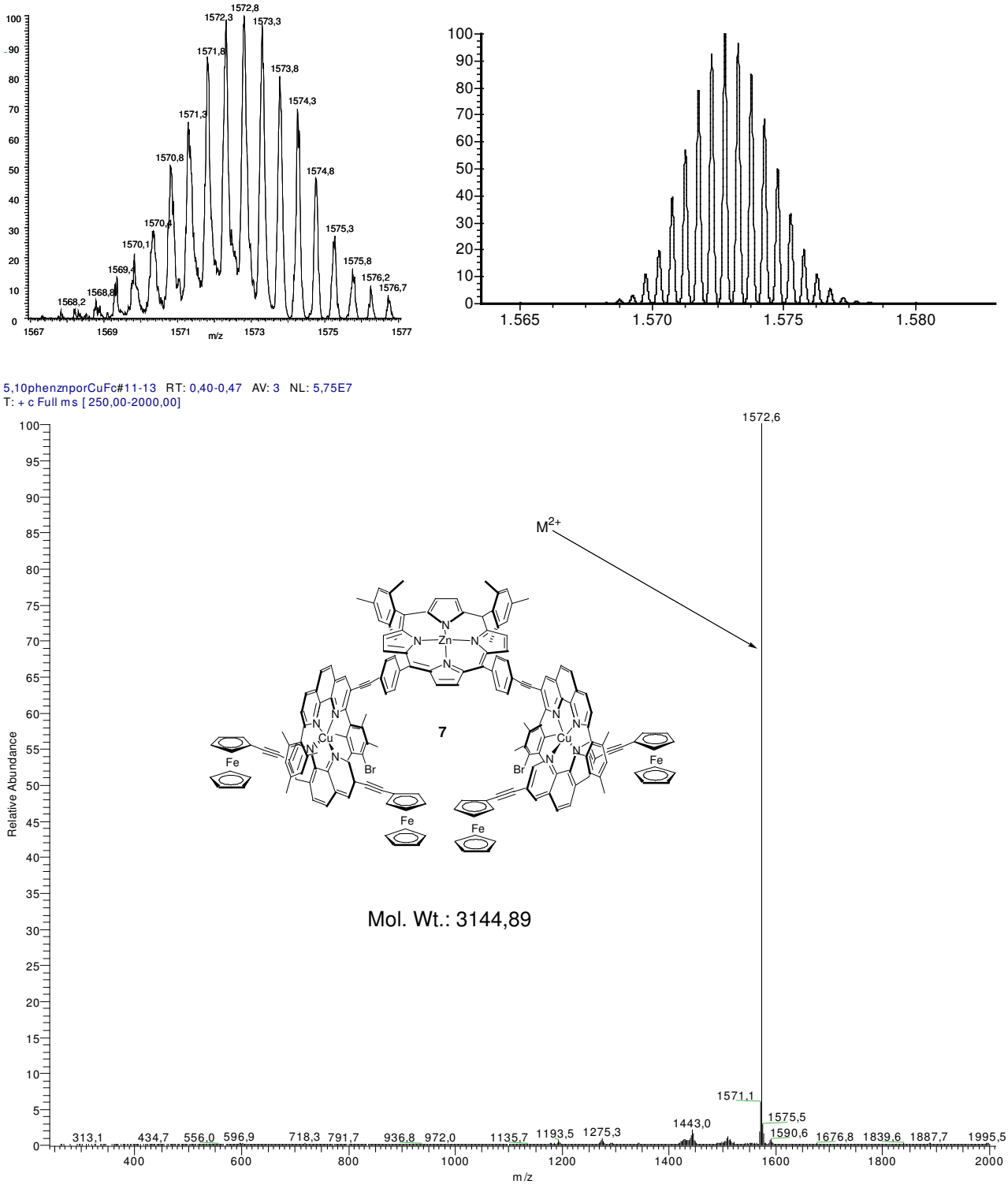

5,10phenznporCuFc#11-13 RT: 0,40-0,47 AV: 3 NL: 5,75E7
T: + c Full ms [250,00-2000,00]

Figure S 9 ESI-MS of **7** showing a M^{2+} signal at about m/z = 1573. Top left: isotopic splitting pattern recorded for M^{2+} of **7**. Top right: Simulated isotopic splitting pattern for M^{2+}.

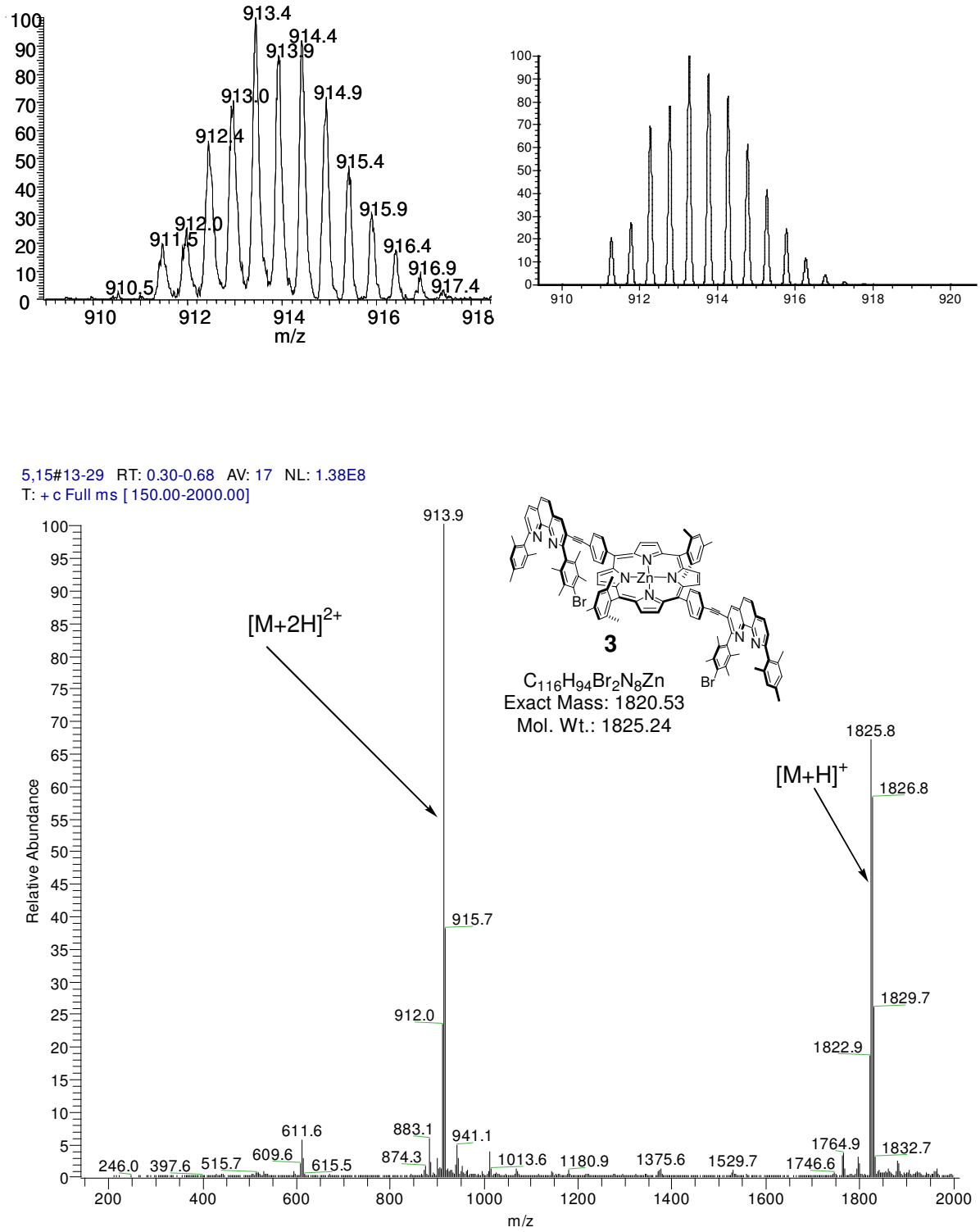

Figure S 10 ESI-MS of **3** showing the $[M+H]^+$ and $[M+2H]^{2+}$ signals. Top left: isotopic splitting pattern recorded for $[M+2H]^{2+}$ of **3**. Top right: Simulated isotopic splitting pattern for $[M+2H]^{2+}$.

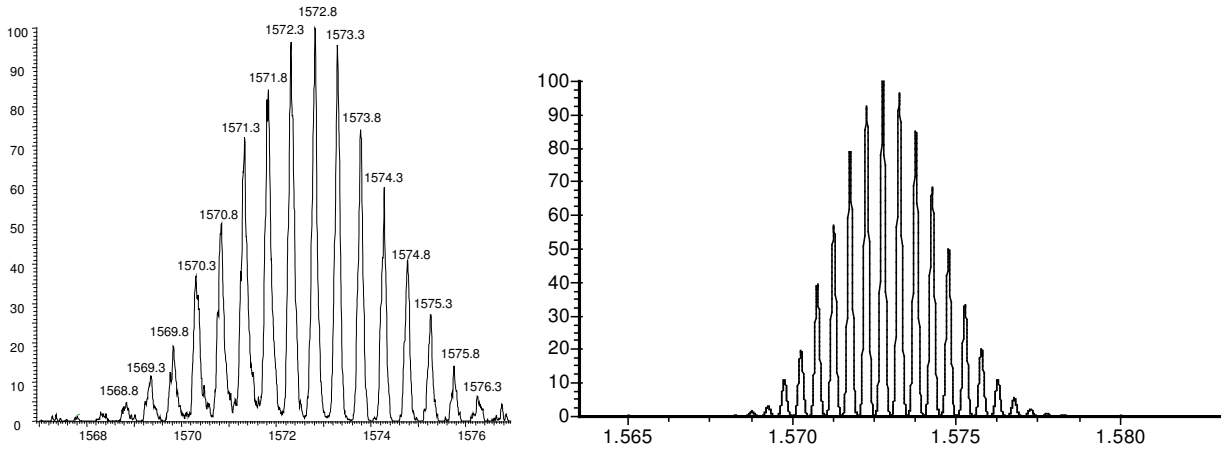

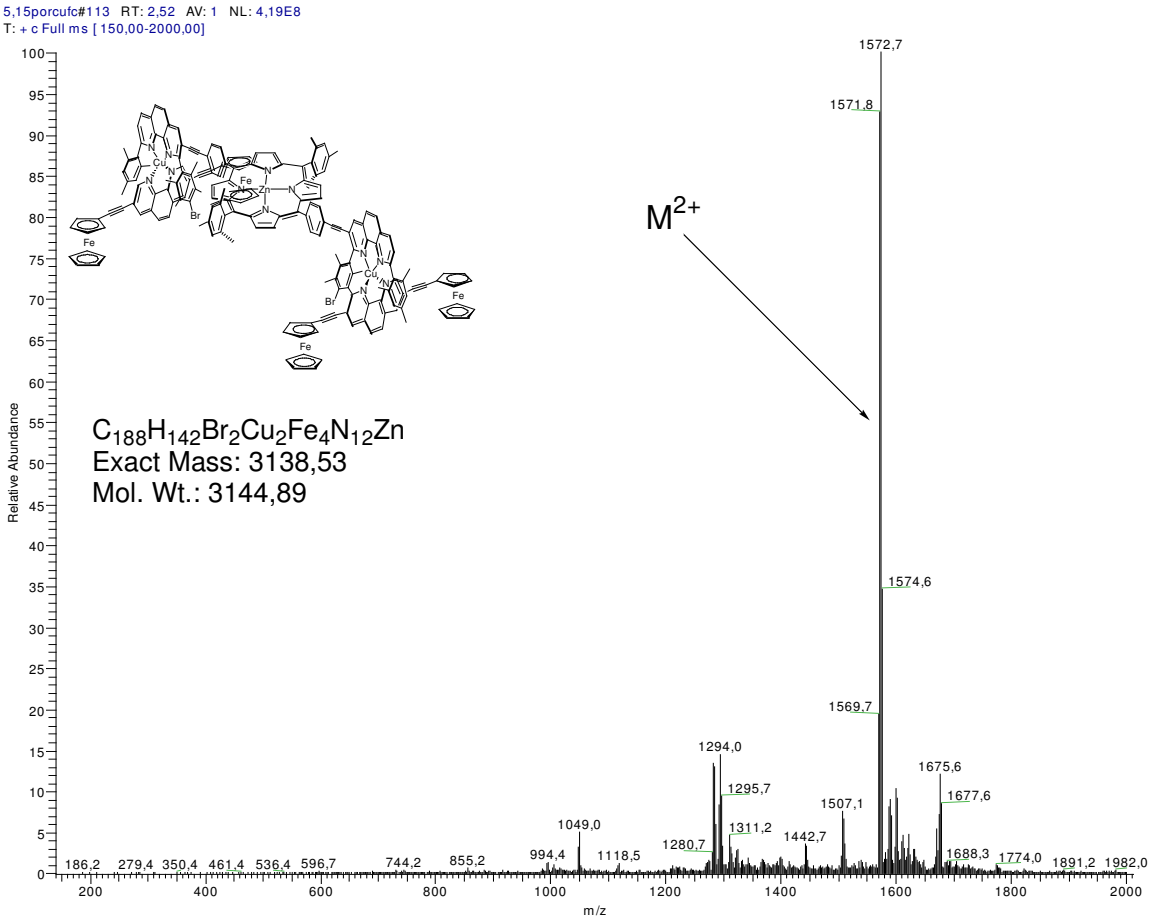

Figure S 11: ESI-MS of **8** showing the M^{2+} signal at about m/z = 1573. Top left: isotopic splitting pattern recorded for M^{2+} of **8**. Top right: Simulated isotopic splitting pattern for M^{2+}.

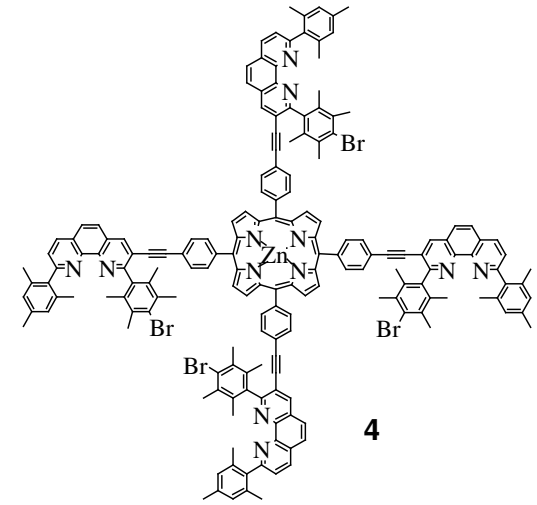

4

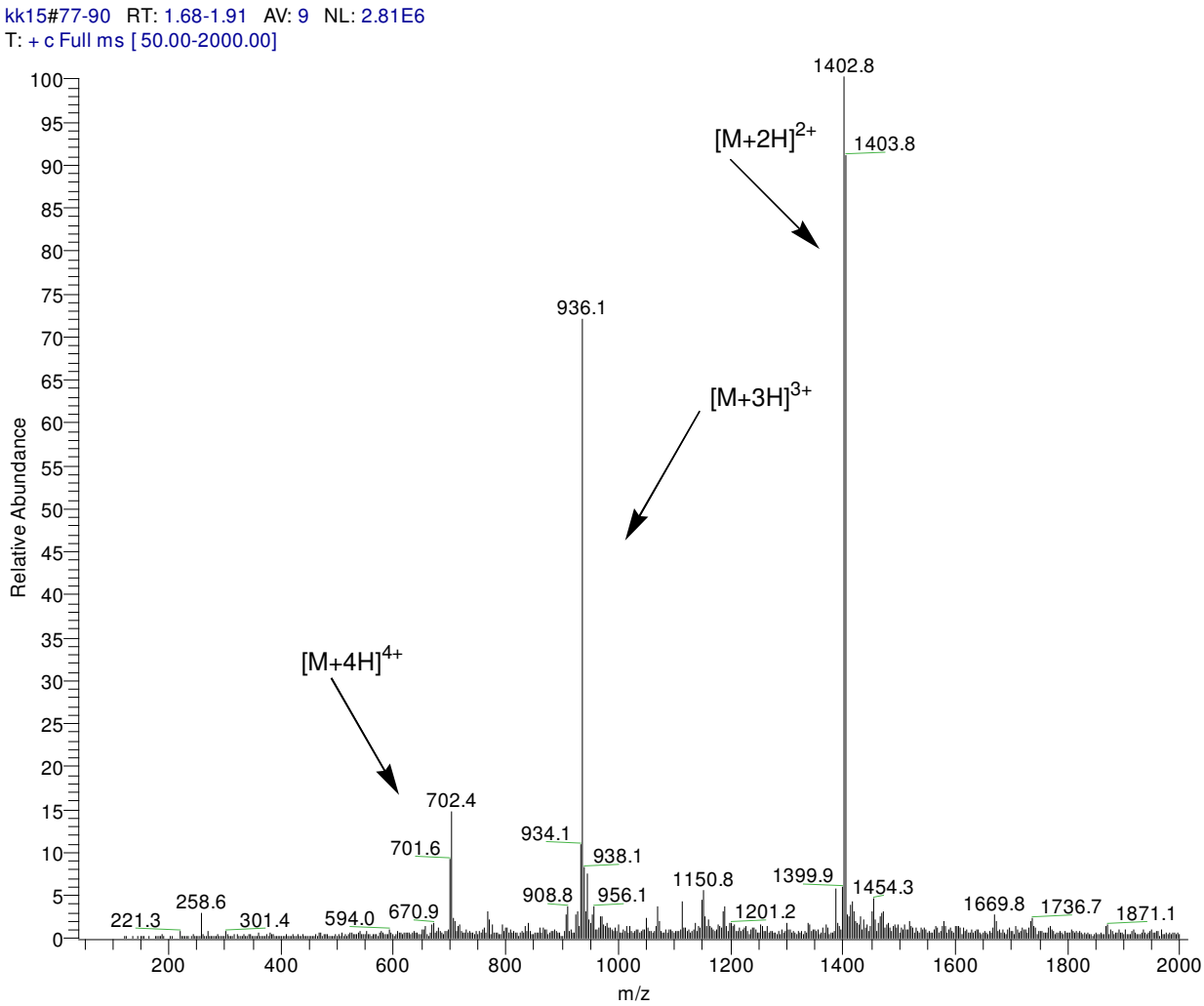

Figure S 12: ESI-MS of **4** showing the $[M+4H]^{4+}$, $[M+3H]^{3+}$ and $[M+2H]^{2+}$ signals.

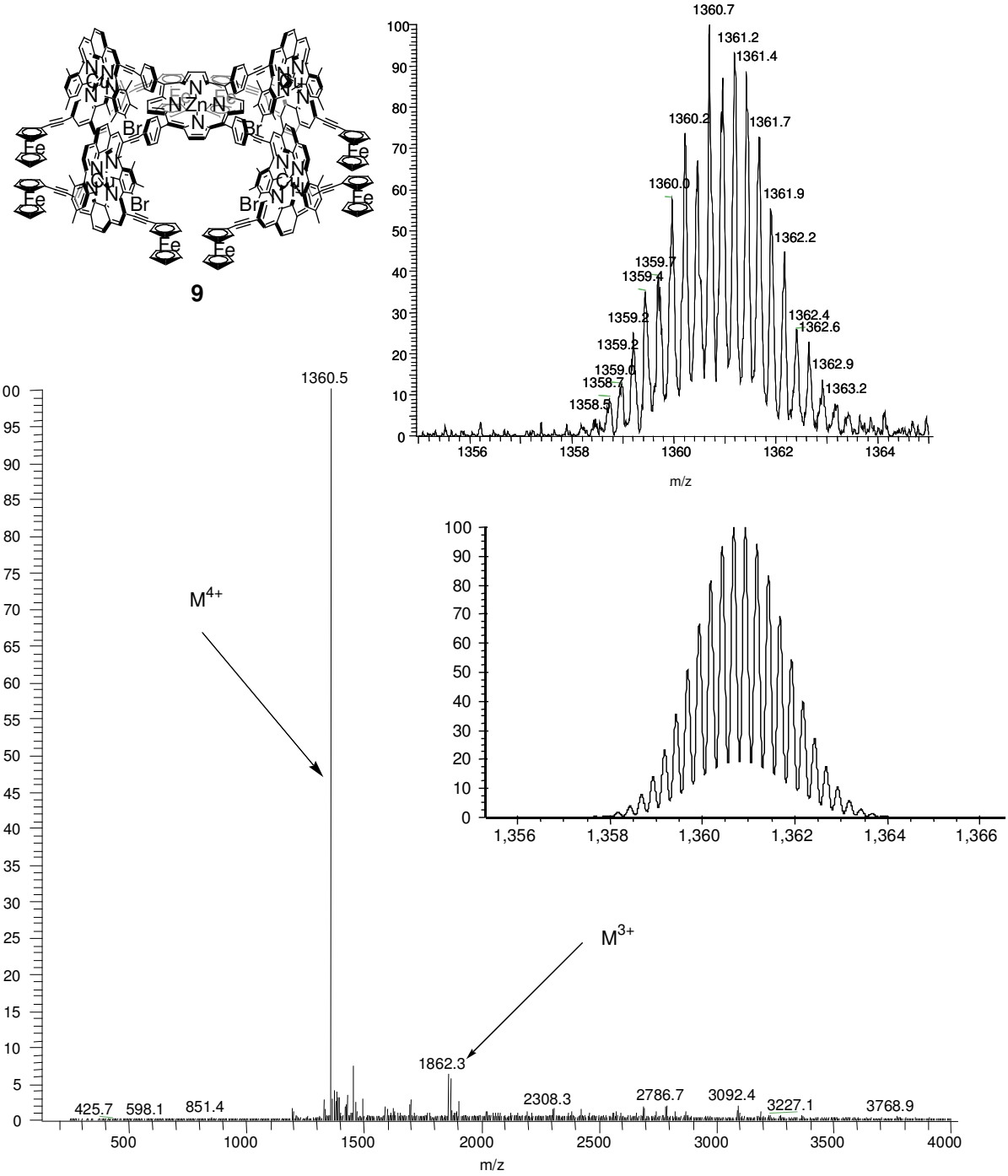

Figure S 13 ESI-MS of **9** showing the M^{4+} and M^{3+} signals. Inset top: isotopic splitting pattern recorded for M^{4+} of **8**. Inset bottom: Simulated isotopic splitting pattern for M^{4+}.

3. Cyclic voltammetry and DPV

Cyclic voltammetry was measured on a Parstat 2273 in dry dichloromethane or dichloroethane in 0.1 M nBu$_4$NPF$_6$ electrolyte solution against a Ag wire as a quasi-reference electrode and dimethyl ferrocene as internal standard at 100 mVs^{-1} scan rate. Differential pulse voltammetry was measured in dichloroethane with 0.1 M nBu$_4$NPF$_6$ as supporting

electrolyte. Experimens were performed with a scan rate of 10 mV s^{-1} and a pulse height of 2 mV for a duration of 50 ms. The concentration of the complexes **11-14** were maintained at~ 0.5 mM for the measurements.

Table S 3 Redox potentials of compounds **1-4, 6-9**, and **11-14** measured by DPV in dichloroethane *vs*. dimethylferrocene (DMFc). To obtain values against the more common ferrocene redox couple, please subtract 0.09 V from the values against DMFc.

	$E_{1/2}$ *vs*. DMFc[c]						HOMO-LUMO (eV)[e]
	$P^{+/2+}$	$P^{0/+}$ $Cu^{+/2+}$	$Fc^{0/+}$	$C_{60}{}^{0/-}$	$C_{60}{}^{-/2-}$	$P^{0/-}$	
1[a]	0.79	0.43				−1.85	
2[a]	0.85	0.49				−1.76	
3[a]	0.86	0.48				−1.74	
4[a]	0.82	0.55				−1.66	
6[b]	0.83	0.50, 050	0.30			−1.82	
6a	0.83	0.50	0.30				
7[b]	0.86	0.50, 050	0.29			−1.77	
8[b]	0.83	0.50, 050	0.30			−1.77	
9[b]	0.86	0.50, 050	0.29			−1.75	
11[b]	0.94	0.46, 0.39[d]	0.30[d]	–0.97	–1.38	–1.89	1.27
12[b]	0.92	0.51, 0.45[d]	0.30	–0.95	–1.35	–1.79	1.25
13[b]	0.86	0.48, 0.42[d]	0.29	–0.99	–1.41	–1.79	1.28
14[b]	0.90	0.49, 0.37[d]	0.28	–0.95	–1.35	–1.76	1.23

[a] Determined by cyclic voltammetry in CH_2Cl_2 with ferrocene as internal standard, referenced to the dimethylferrocene couple (DMFc). [b] Determined by DPV in dichloroethane with NBu_4PF_6 as electrolyte with DMFc as internal standard. [c] Measured at 100 mV s^{-1}. All potentials are referenced against dimethylferrocene redox couple. [d] Obtained by deconvolution. [e] Determined from the redox potentials $Fc^{0/+} - C_{60}{}^{0/-}$.

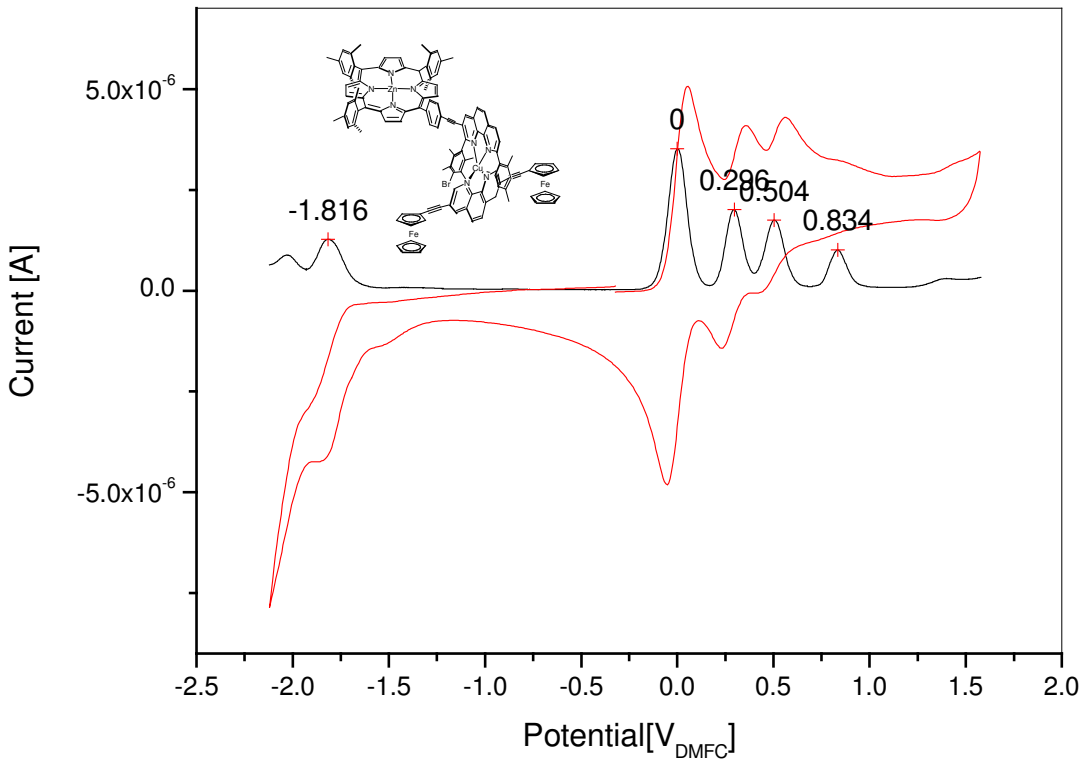

Figure S 14 CV and DPV of **6** measured in DCE with dimethyl ferrocene as the standard and nBu_4NPF_6 as the electrolyte

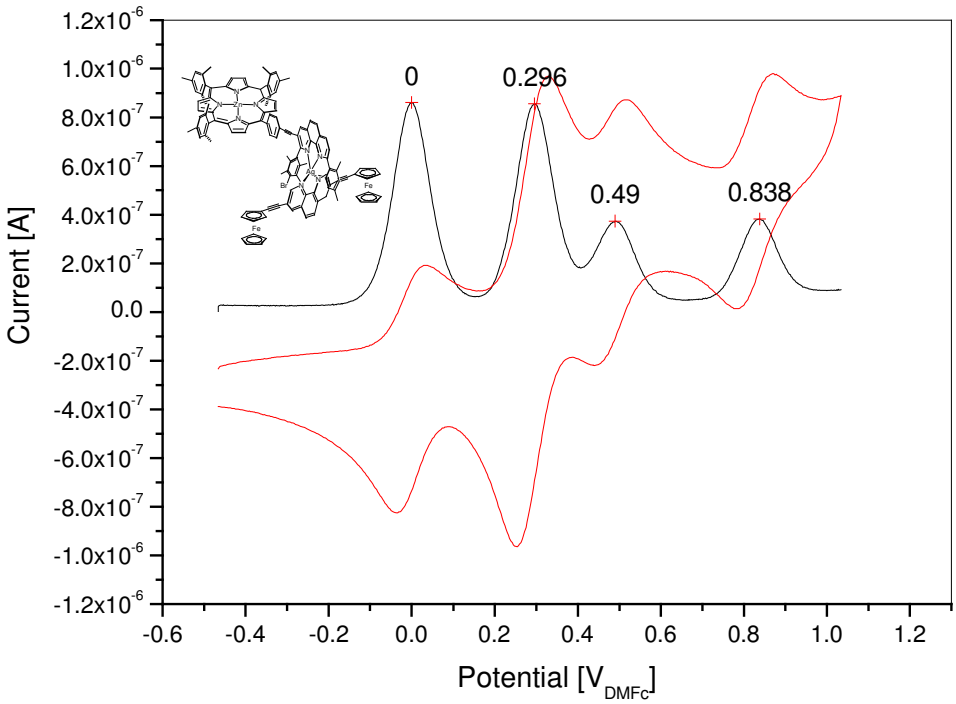

Figure S 15: CV and DPV of **6a** measured in DCE with dimethyl ferrocene as the standard and nBu_4NPF_6 as the electrolyte

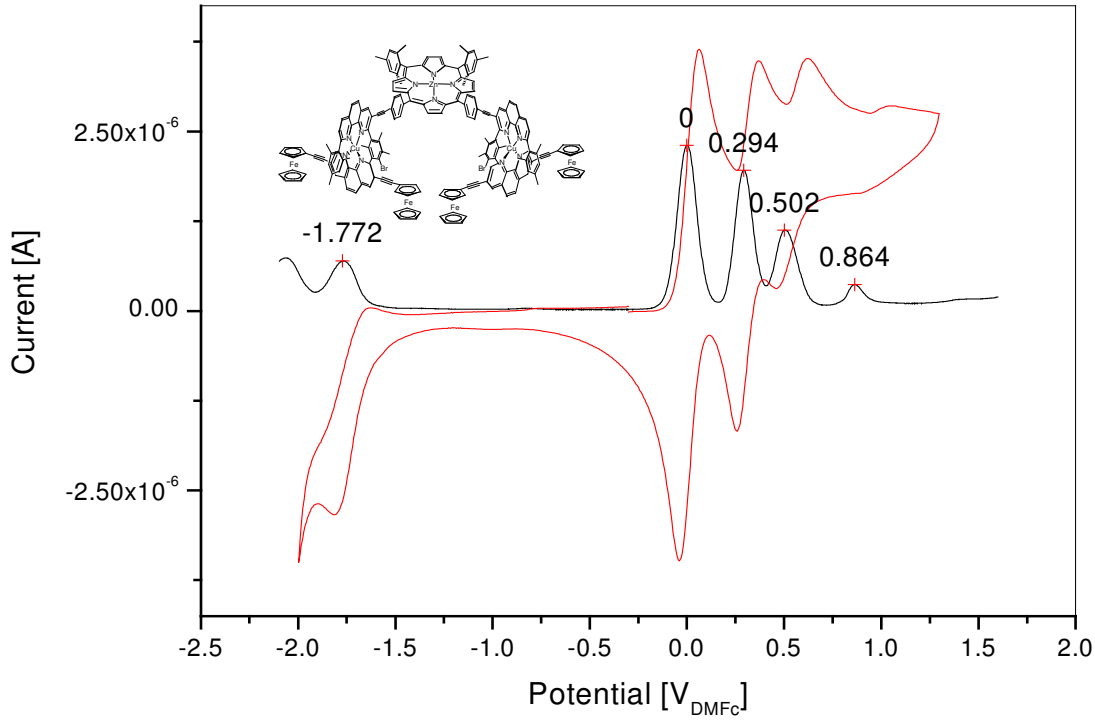

Figure S 16 CV and DPV of **7** measured in DCE with dimethyl ferrocene as the standard and nBu_4NPF_6 as the electrolyte

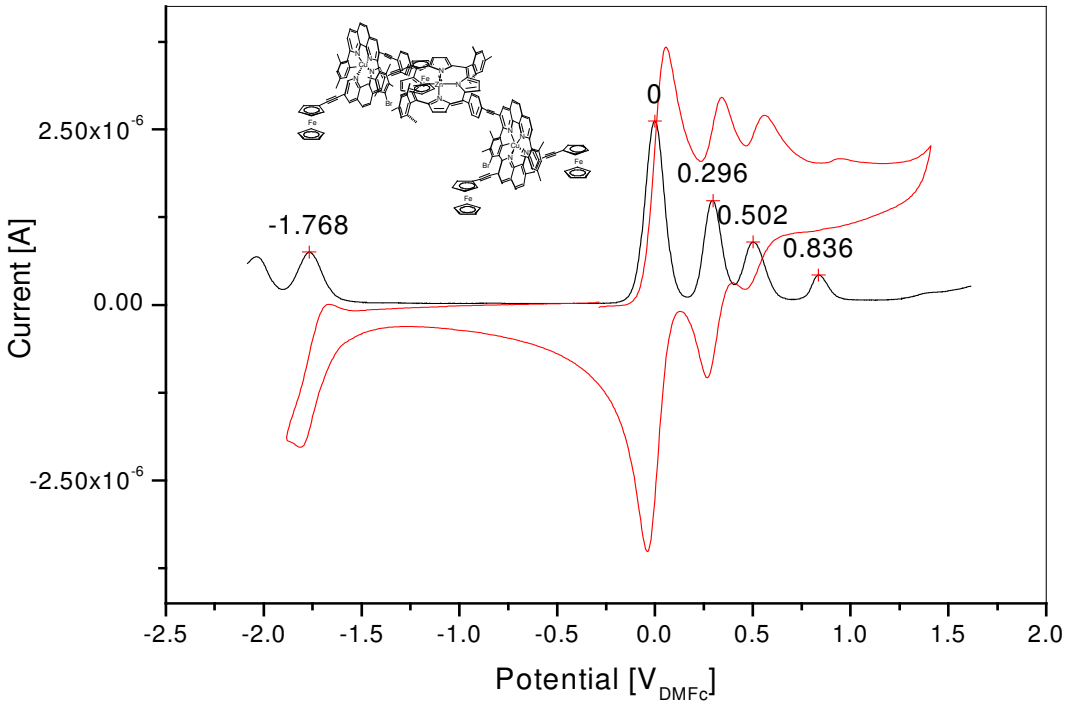

Figure S 17 CV and DPV of **8** measured in DCE with dimethyl ferrocene as the standard and nBu_4NPF_6 as the electrolyte

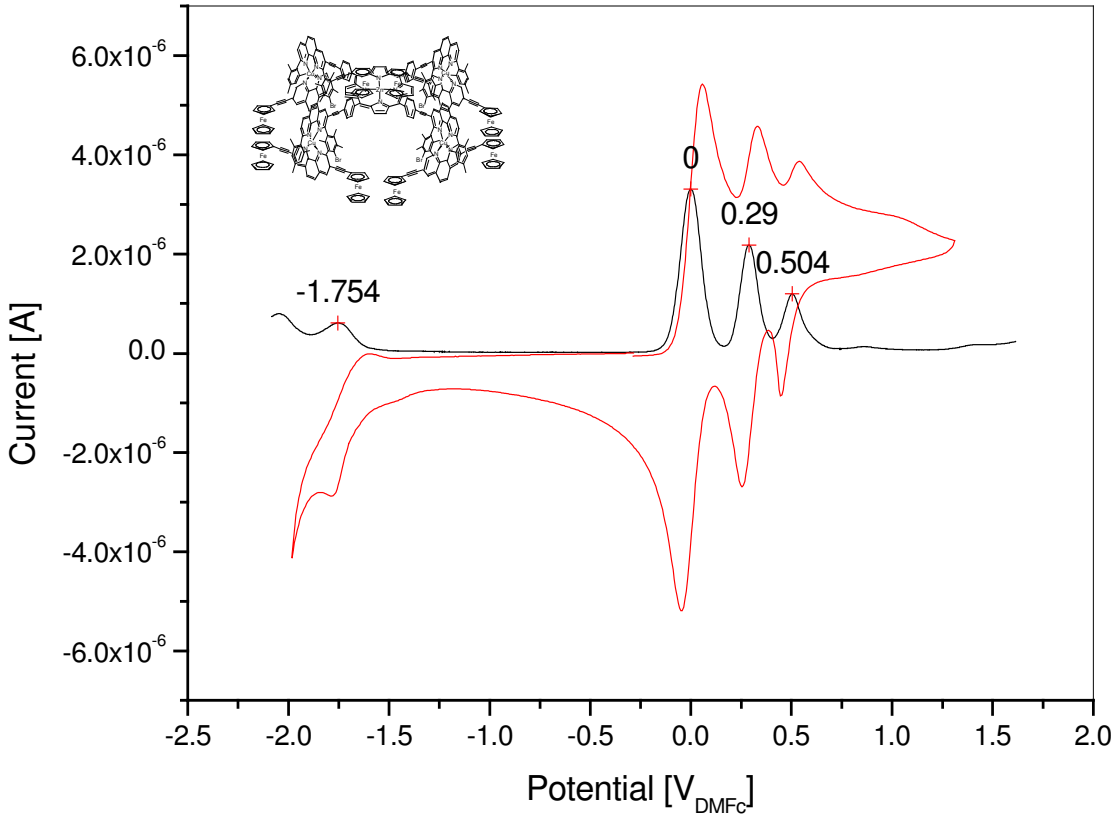

Figure S 18 CV and DPV of **9** measured in DCE with dimethyl ferrocene as the standard and nBu_4NPF_6 as the electrolyte.

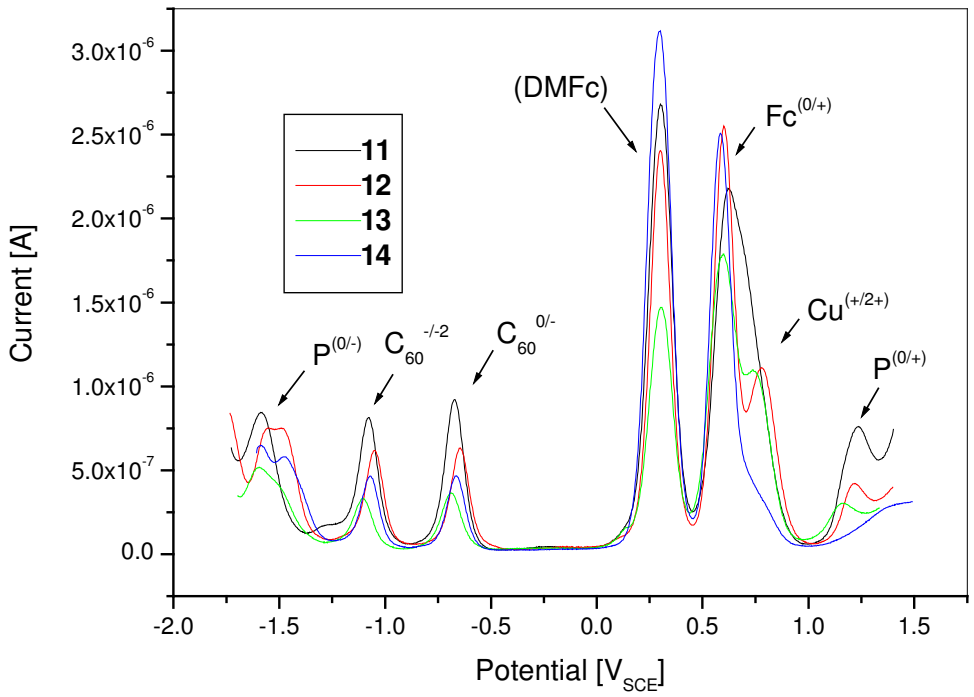

Figure S 19 DPV plots (vs SCE) of **11**-**14** measured in dichloroethane with dimethyl ferrocene as the standard and nBu_4NPF_6 as the electrolyte.

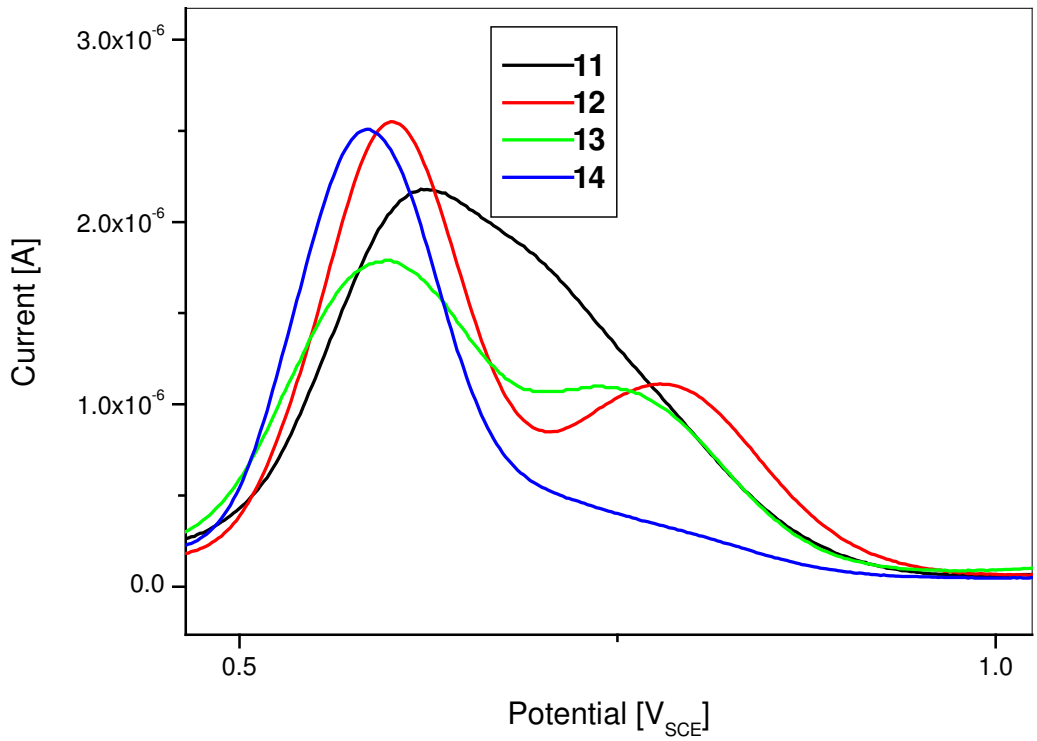

Figure S 20 Peaks corresponding to ferrocene and Cu(I)/$P^{0/+}$ oxidation from the DPV plots of **11-14** (vs SCE). Inset: Deconvolution of the peak of **11** performed by PEAKFIT.

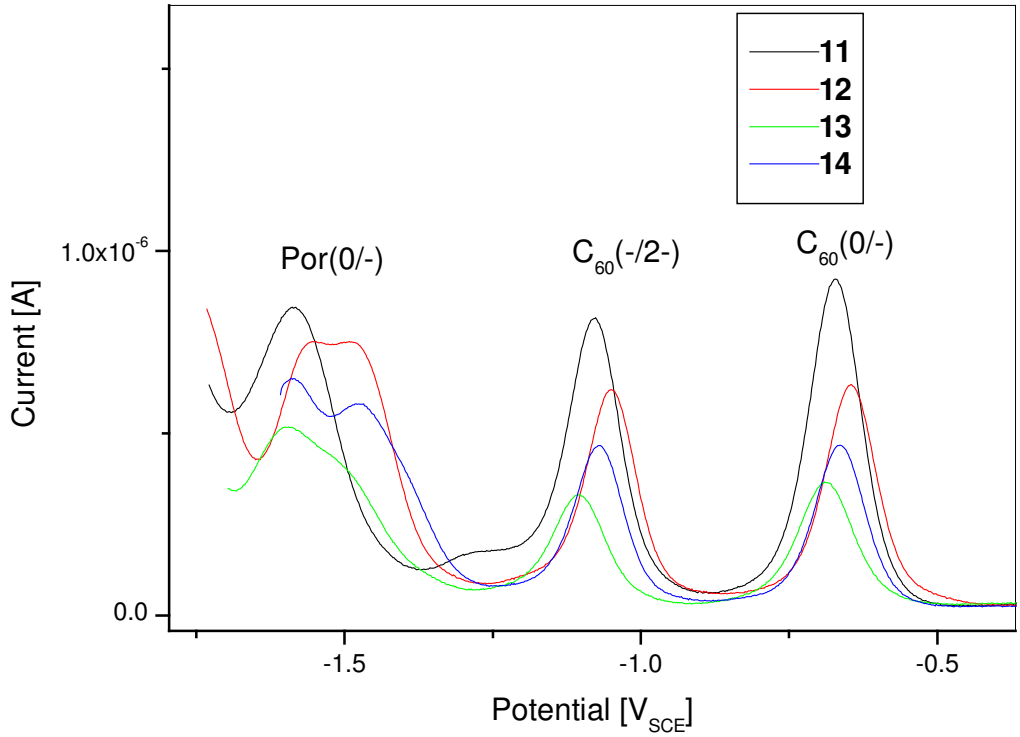

Figure S 21 Selected parts from the DPV curves (vs SCE) from **11-14** representing the peaks corresponding to the reduction of the porphyrins and C_{60}.

4. UV Titrations

UV titrations were carried out by adding 10 µL aliquots of a 1 mM solution of **10** in DCE to a 0.001 mM solution of the aggregates **6-9** in a quartz cuvette at 25 °C. The spectra were recorded on a Cary 300 double beam spectrophotometer. The data obtained from the UV/Vis titrations were analysed by fitting the whole series of spectra at 0.5-nm intervals using the software SPECFIT[1] version 3.0.22 (Spectrum Software Associates, P.O. Box 4494, Chapel Hill, NC 27515-4494, USA), which uses a global analysis system with expanded factor analysis and a Marquardt least-squares minimization to obtain globally optimized parameters.

[1] (a) M. Maeder, and A. D. Zuberbühler, *Anal. Chem.* 1990, **62**, 2220; (b) H. Gampp, M. C. J. Maeder, and A. D. Zuberbühler, *Talanta* 1986, **33**, 943.

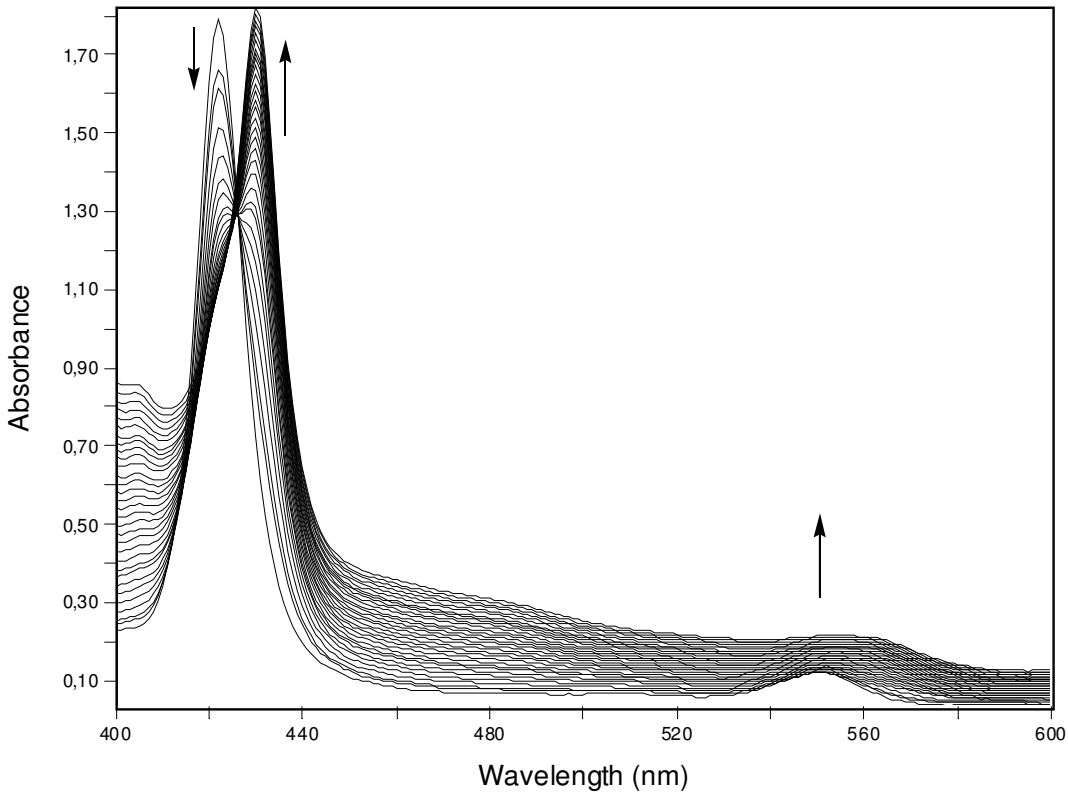

Figure S 22 UV-vis spectral changes observed during the titration of **6** (4.18μM) with **10** (30 aliquots of 10 μL each of a 0.11mM solution) in DCE at 298K.

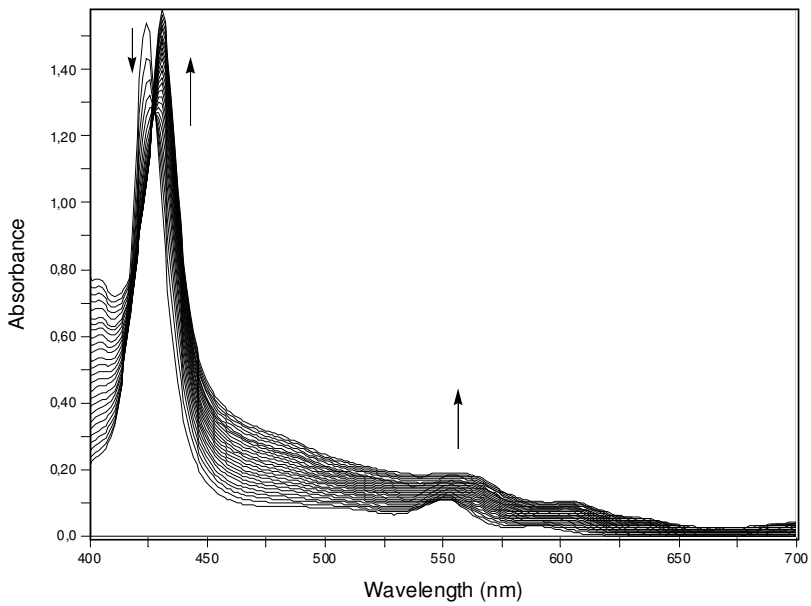

Figure S 23 UV-vis spectral changes observed during the titration of **7** (3.43μM) with **10** (26 aliquots of 10 μL each of a 0.11mM solution) in DCE at 298K.

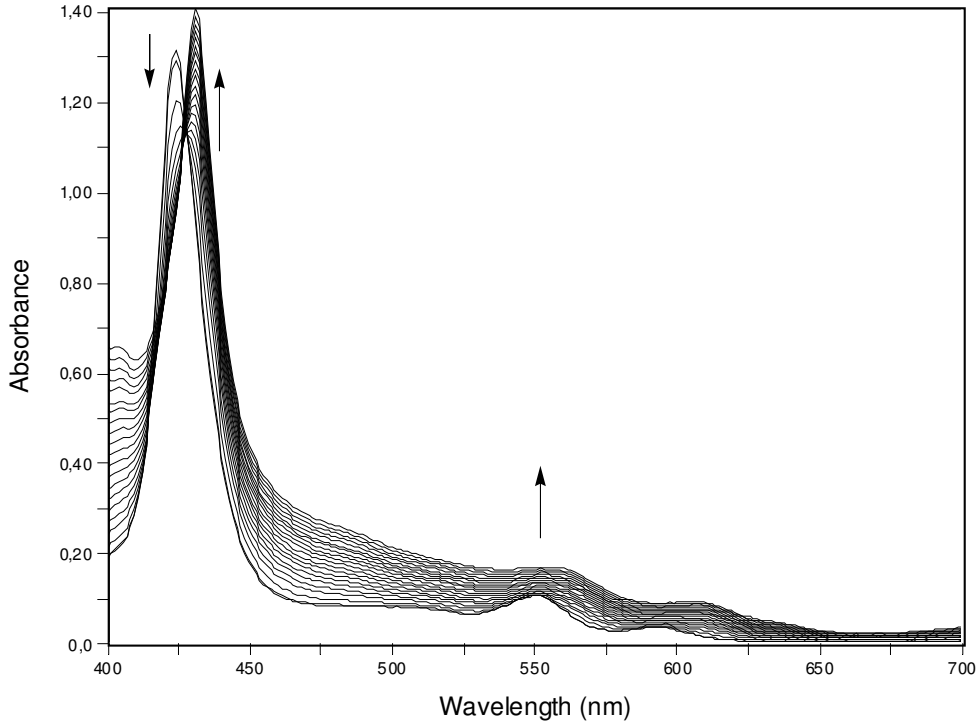

Figure S 24 UV-vis spectral changes observed during the titration of **8** (3.08μM) with **10** (20 aliquots of 10 μL each of a 0.11mM solution) in DCE at 298K.

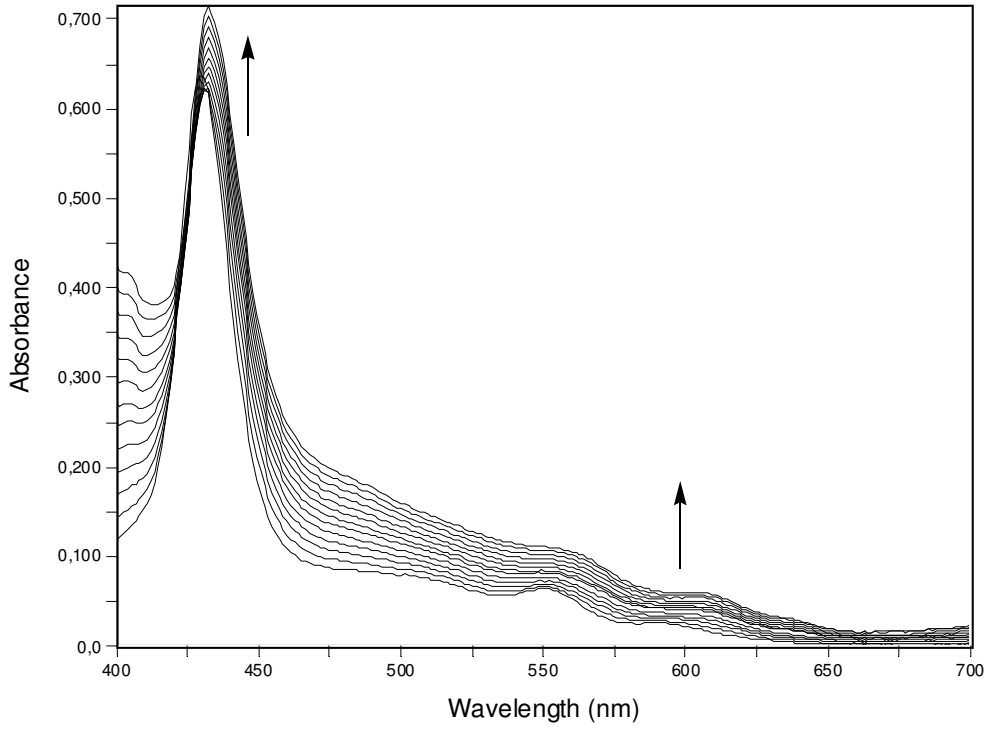

Figure S 25 UV-vis spectral changes observed during the titration of **9** (1.55μM) with **10** (12 aliquots of 10 μL each of a 0.11mM solution) in DCE at 298K.

5. Crystal packing of 5

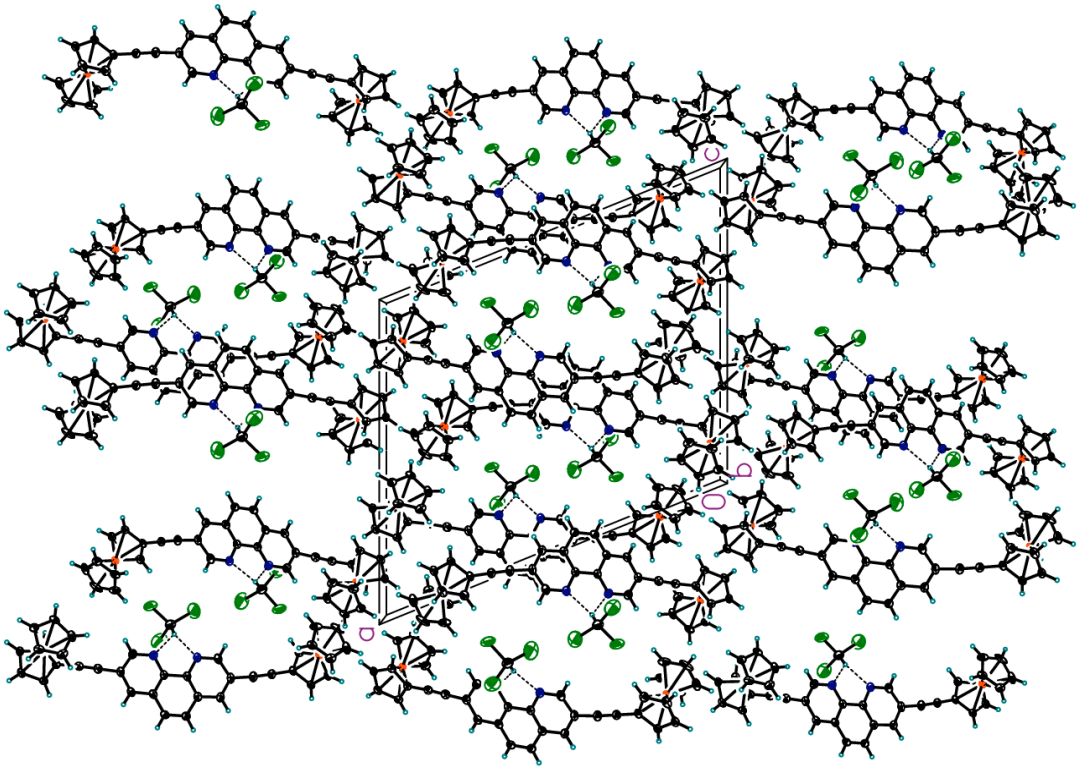

Figure S 26: Crystal packing of **5** displaying phenanthroline stacks along the b direction and partially overlapping π systems**.**

6. PM3 model of 11

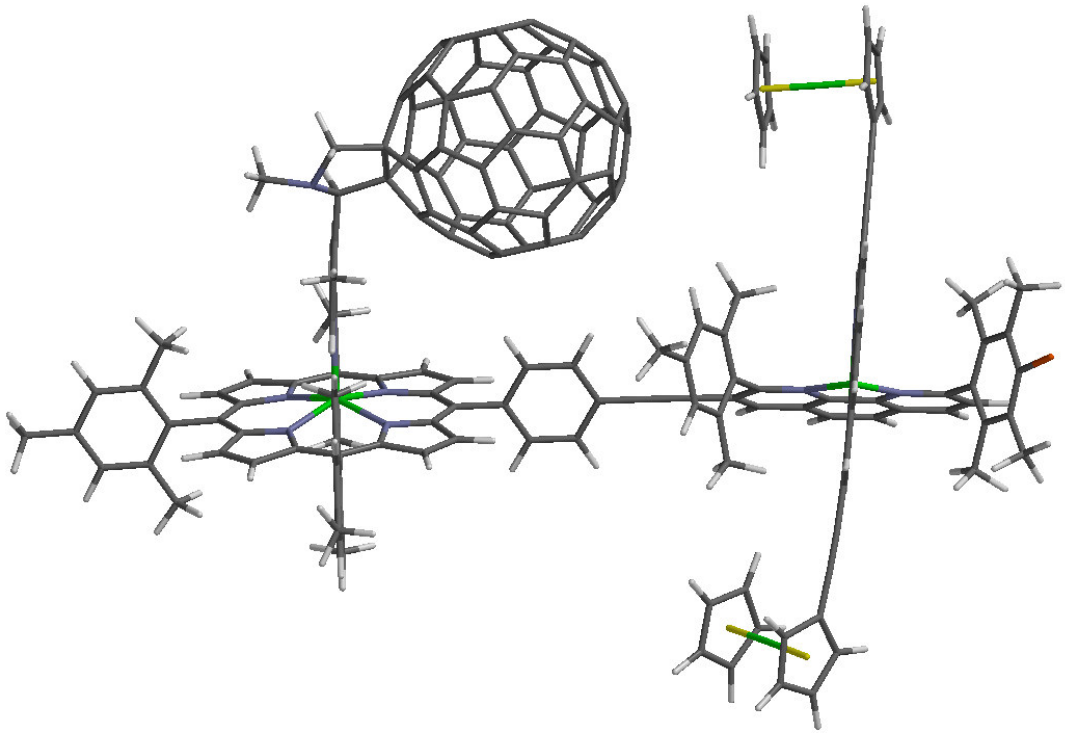

Figure S 27 PM3 minimized structure (SPARTAN) of **11** showing the fullerene and ferrocenyl unit in almost van der Waals contact.